Concentration dependence of the local electronic properties of AlCuFe quasicrystals and crystalline approximants

1994 J. Phys.: Condens. Matter 6 11189

(http://iopscience.iop.org/0953-8984/6/50/026)

J. Phys.: Condens. Matter 6 (1994) 11189–11209. Printed in the UK

Concentration dependence of the local electronic properties of AlCuFe quasicrystals and crystalline approximants

F Hippert†, R A Brand‡, J Pelloth‡ and Y Calvayrac§

† Laboratoire de Physique des Solides, associé au CNRS, Batiment 510, Université de Paris Sud, F-91405 Orsay Cédex, France

‡ Laboratorium für Angewandte Physik, Universität Duisburg, D-47048 Duisburg, Germany

§ CECM/CNRS, 15 rue G Urbain, F-94407 Vitry Cédex, France

Received 4 August 1994, in final form 6 October 1994

Abstract. The icosahedral quasicrystal $Al_{100-x-y}Cu_xFe_y$ is stable at low temperature only along a narrow line-like domain around $Al_{62}Cu_{25.5}Fe_{12.5}$. In a nearby narrow line-like domain parallel to the first, the icosahedral structure transforms at low temperatures into a stable rhombohedral approximant (3/2) phase. For the first time, we have investigated the local electronic properties and local order *along these stability lines*, using both ^{57}Fe Mössbauer and ^{27}Al NMR spectroscopy. We show that the local properties (as given by the ^{57}Fe central line shift and quadrupole splitting and ^{27}Al average line shift and line shape) are *insensitive* to the nature of the long-range order, icosahedral quasicrystal or rhombohedral approximant, at a given composition. In addition, a new pentagonal approximant found along the rhombohedral line gave the same results as the quasicrystal for the same composition. The changes in the electronic properties along the two stability lines are about a factor of three *smaller* than the changes from the stable icosahedral to the stable rhombohedral domains although there is a factor of three *larger* change in concentration. These observations are consistent with the constant value of the number of electrons per atom (referred to as e/a) along the lines, and changes in e/a between them, as estimated from the alloy composition.

1. Introduction

The structural and electronic properties of the quasicrystalline phases have attracted much attention recently. Thermodynamically stable icosahedral quasicrystalline (QC) alloys have been found in regions of ternary phase diagrams such as AlCuFe, AlLiCu and AlPdMn showing very complex phase structures. Among the many crystalline phases with compositions close to the QC ones, crystalline approximant phases [1] are especially interesting, as their diffraction pattern and their local order are very similar to those of the QC phase. The stable QC phases exhibit surprising electronic properties for alloys composed of good metals, such as a high resistivity with a negative temperature coefficient and a pseudogap at the Fermi level [2, 3, 4]. The electronic properties of the approximants were found to be very close to those of the stable QC phases [2, 5, 6, 7]. Band structure calculations of the periodic approximants [8] indeed show a pseudogap.

Stable QC phases only exist in very narrow composition regions of these ternary phase diagrams. The question arises of whether this behaviour has anything to do with the electronic properties of such systems. In Hume-Rothery alloys, the strong diffraction of electrons at the Fermi level by Bragg planes leads to a pseudogap located at the Fermi energy and an increased stability [9]. It has been argued that similar effects could explain

0953-8984/94/5011189+21$19.50

the pseudogap in stable quasicrystals and approximants and also play a role in the stability of such phases [3, 10].

The AlCuFe quasicrystalline system has been very well characterized with respect to the composition range and thermal behaviour [11, 12, 13]. It is possible to produce samples which are single phase with reproducible properties. At high temperatures (~700 °C), the icosahedral phase (hereafter ico) exists in a broad region of composition. At lower temperatures, it is found that the existence domain of the ico quasicrystalline phase is reduced to a narrow composition strip, which can be nearly approximated by a line, hereafter called the i-line, extending from (24.4, 13.0) to (26.0, 12.2) [13]. Here and in the following, the Cu (x) and Fe (y) concentrations in at.% are given as (x, y). The extension of the existence domain perpendicular to this line appears to be negligible. For samples belonging to this domain, long annealing at intermediate temperatures does not lead to any further changes in the x-ray diffraction lines [11]. In the following, we will take this as an indication that along this line, the ico phase is the stable structure at low temperatures.

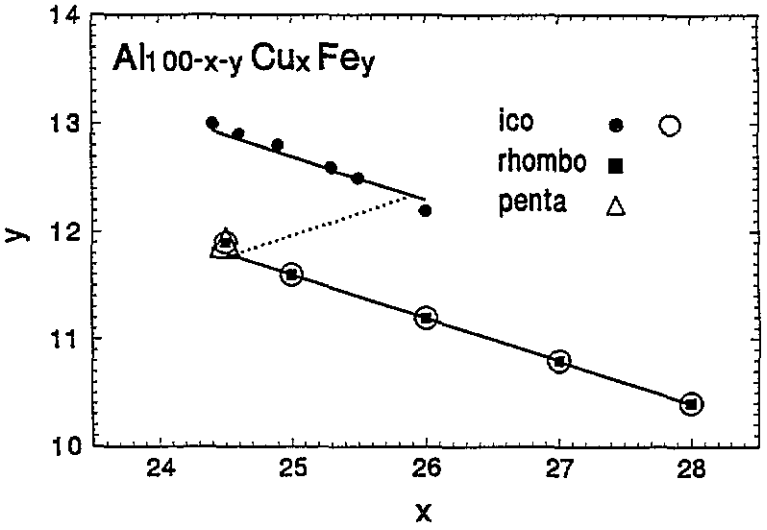

Figure 1. Schematic concentration diagram showing the $Al_{100-x-y}Cu_xFe_y$ samples studied in the present work. Solid symbols refer to stable states at low temperature (LT). Open symbols refer to metastable states at LT. We have selected six stable icosahedral samples spanning the LT stability domain of the ico phase (solid circles) and five stable rhombohedral samples spanning the LT stability domain of the rhombo phase (solid boxes). For these later five compositions a LT metastable ico state can be obtained (open circles) and for one composition (24.5, 11.9), a LT metastable pentagonal state (open triangle) as well. Also shown are the lines at constant average number of valence electrons per atom (see section 5) for the stable ico phase and for the stable rhombo phase (solid lines). The dotted line connects ico states with constant lattice parameter ($a_{6D} = 6.316$ Å, *see section 5*).

Several investigations of the phase diagram of the $Al_{100-x-y}Cu_xFe_y$ system, in the vicinity of the ico QC phase, have been performed. A crystalline rhombohedral 3/2 approximant phase (hereafter rhombo) was first observed by transmission electron microscopy and x-ray investigations [14]. Later, the stability domain of this phase was studied as a function of temperature [13]. Surprisingly enough it was recently found that the low-temperature stability domain of the rhombo phase is also a narrow line, hereafter called the r-line, and is parallel to the i-line, extending from (24.5, 11.9) to (28.0, 10.4) [15, 16].

It is interesting to ask whether changes of the electronic properties or the local order occur within each domain and from one domain to the other. In the Hume-Rothery scheme, a possible explanation of the shape of these stability domains would be that they are lines of constant electronic structure. Thus we must find physical parameters sensitive enough to the electronic structure to evidence differences between samples along the two lines which are expected to be quite small in view of the expected similarity in short-range order. Local methods which can separate different contributions (secondary phases, magnetic contributions, etc) are *a priori* better than those which measure only bulk properties. Possibilities in the case of the AlCuFe system include ^{57}Fe Mössbauer spectroscopy, as well as ^{27}Al nuclear magnetic resonance (NMR). Both of these methods are also sensitive to the local order. The ^{57}Fe central line shift (isomer shift) and quadrupolar electric field gradient (EFG) give us information on the electronic and chemical structure around the Fe nucleus. In a similar manner, the ^{27}Al Knight shift and quadrupolar EFG give us information on the electronic and chemical structure around the Al nucleus. Thus we have used these two methods to compare samples along the two stability domains. Moreover along the r-line, the ico phase exists at temperatures higher than 710 °C. This ico phase transforms to the rhombo phase by annealing at 710 °C but it can be retained by quenching fast enough to prevent this transformation, producing an ico state which is metastable at low temperature. This fact provides us with a very simple way to check on the possible effect of long-range order on the electronic properties by comparing the same sample material in these two crystallographic states. In addition, it has recently been found that another crystalline approximant with pentagonal symmetry (hereafter penta) exists along this r-line for some compositions, with lower Cu content [15]. One such structure will also be presented.

2. Sample preparation

All the samples used were prepared at CECM by planar flow casting. The procedure used to obtain the as-quenched material was identical to that given in [10]. A major difficulty in this work was to master the alloy preparation in order to obtain samples with compositions accurate to about 0.1 at.%. The phase diagram has such a complexity [12, 13, 16] that tiny changes in composition may generate large differences in the thermal behaviour of these alloys. The reproducibility was checked by preparing each composition several times. The as-quenched samples contain a small amount of the cubic β phase (of the order of a few %), the composition of the ico phase then differing slightly from the nominal composition. This β phase is easily eliminated by subsequent annealing. Also, an appreciable disorder is present in the as-quenched samples, leading to systematic shifts of the observed Bragg peaks from their calculated positions and to broadening of the diffraction peaks. The samples used in the present study are listed in table 1 with a short description of the heat treatment applied to the as-quenched material. Here and in the following, stable or metastable will refer to low-temperature stability (LT). The samples have all been characterized by x-ray diffraction. The measured six-dimensional (6D) lattice parameter a_{6D} is included in this table, as well as the lattice parameter a_{Rh} of the rhombo state. The samples were all found to be single phase to within the accuracy of the x-ray diffraction measurements ($\sim$ 1%). Typical diffraction patterns can be found in [13] and [15]. A schematic concentration diagram is shown in figure 1. The six stable ico samples (along the i-line) and the five rhombohedral samples (along the r-line) studied here span the whole of the known low-temperature stability ranges of the ico and of the rhombo phases [11, 12]. In figure 1 the extension of the stability domains perpendicular to these lines is negligible. In addition, these same samples on the r-line were prepared in the LT metastable ico state by quenching (see table 1). One of these samples

Table 1. Samples studied including Cu and Fe concentrations, the nature of the long-range order, the heat treatment, starting from the as-quenched flakes (with the exception of sample Q), and the lattice parameters a_{6D} for ico and a_{Rh} for rhombo. Stable and metastable refer to low temperature (LT).

Sample	% Cu	% Fe	Lattice parameter A–K, R: a_{6D} M–P: a_{Rh} (Å)		Heat treatment and resulting state
A	24.4	13.0	6.3198	A–F:	2 h at 800 °C. Cooling rate not important. Results in an icosahedral phase stable at low temperature (LT).
B	24.6	12.9	6.3193		
C	24.9	12.8	6.3180		
D	25.3	12.6	6.3173		
E	25.5	12.5	6.3176		
F	26.0	12.2	6.3153		
G	24.5	11.9	6.3168	G–	2 h at 740 °C. Quenched in quartz capsule. Results in an icosahedral phase stable at 740 °C but metastable at LT.
H	25.0	11.6	6.3149	K:	
I	26.0	11.2	6.3125		
J	27.0	10.8	6.3108		
K	28.0	10.4	6.3088		
L	24.5	11.9	—	L:	11 d at 670 °C. Cooling rate not important. Stable rhombohedral phase.
M	25.0	11.6	32.1604	M–	3 d at 705 °C. Cooling rate not important. Results in a stable rhombohedral phase at LT.
N	26.0	11.2	32.1511	P:	
O	27.0	10.8	32.1393		
P	28.0	10.4	32.1273		
Q	24.5	11.9	—	Q:	Heat treatment as in sample L. Subsequent anneal for 9 d at 705 °C. Results in a pentagonal phase stable at 705 °C but metastable at LT.
R	24.5	12.5	6.3208	R:	2 h at 800 °C. Quenched in quartz ampoule. Results in icosahedral phase stable at 800 °C but metastable at LT (two-phase region at LT: ico plus rhombo).

was also prepared in the newly discovered penta approximant state metastable at LT.

The stable ico samples at LT, A–F (sample labels are given in table 1), exhibit a very high degree of icosahedral long-range order. Within the accuracy of the high-resolution x-ray spectra, the Bragg peak positions coincide with the calculated ones and no broadening

is observed [11, 13]. On the other hand, for samples belonging to the LT stability domain of the rhombo phase, the ico state, which is obtained by quenching and is metastable at LT, always contains some defects as broadened Bragg peaks are always observed. Details on the phase diagram and on the nature of the transformations from the rhombo state to the ico or penta states can be found in [15].

There is some confusion in the literature on the heat treatment which is necessary to produce the rhombo state, so that great care is necessary. In the view of the information on the phase diagram and the phase transformations now available [13, 15], it appears that the heat treatments applied to the icosahedral state to obtain a rhombohedral state in several different previously published papers (for example 24 h at 600 °C for $Al_{63}Cu_{25}Fe_{12}$ in [17] and 50 h at 650 °C in $Al_{65}Cu_{23}Fe_{12}$ in [18]) were insufficient to achieve the transformation. The final samples obtained after annealing, claimed to be rhombohedral in these papers, were certainly in an intermediate state of transformation and probably not much different from the starting ico sample. Indeed, only broadened Bragg peaks at the icosahedral QC positions were observed in [18] and not the typical line splitting of the rhombohedral phase [13]. It is not known whether this result was due to a lack of resolution or whether the rhombo phase was not formed. There is also some confusion on the composition range of the low-temperature-stable ico state. The $Al_{65}Cu_{20}Fe_{15}$ alloy composition, widely studied in the first Mössbauer studies [19], is now known to lie in the two-phase region composed of the ico phase and the λ phase [13].

3. ^{57}Fe Mössbauer data

3.1. Spectra and numerical exploitation

The Mössbauer spectra were taken in conventional transmission geometry. All texture effects have been eliminated by reducing the flakes to a fine powder and mixing them with a powder of boron nitride (BN). Several samples have been measured in magic angle geometry (with an angle of $\theta = 54.7°$ between the sample normal and the γ-ray direction) simulating in any event a powder spectrum [20]. No changes were found in such spectra showing that there were no crystallite texture effects present. A short report on our first results was given in [21]. All the spectra discussed here have been remeasured to achieve better accuracy. In order to compare the central line shifts to higher relative accuracy, all spectra were measured on the same system without changing the drive calibration. The spectra presented here were all taken at RT. However, spectra taken at low temperature, and in the presence of a strong external magnetic field (5 T), also show no effects of magnetic order or of significant paramagnetism, as expected from the very low magnetic susceptibility [22]. We do not find any anomalous change in line width between 4.2 K and room temperature, as was reported in [23]. Figure 2 shows several Mössbauer spectra taken at room temperature (only the central part is shown for more detail). The typical broadened asymmetrical quadrupole doublets indicate a broad (quasi-) continuous distribution of local environments with no phases having strongly different hyperfine properties being present. Such spectra are typical for quasicrystalline phases [19, 24], both with respect to the broadened lines, and the apparent line asymmetry. We must consider a combined distribution of quadrupole splitting $\Delta E_Q = \Delta$ and central line shift δ. The simplest general such distribution, $P(\Delta, \delta)$, would be given by a two-dimensional Gaussian form including the two standard deviations σ_Δ and σ_δ, as well as the cross-correlation coefficient between Δ and δ. For such a distribution, lines of equal probability on the Δ–δ plane are ovals with a rotation of the principal axis given by the cross-correlation coefficient. These two standard deviations lead

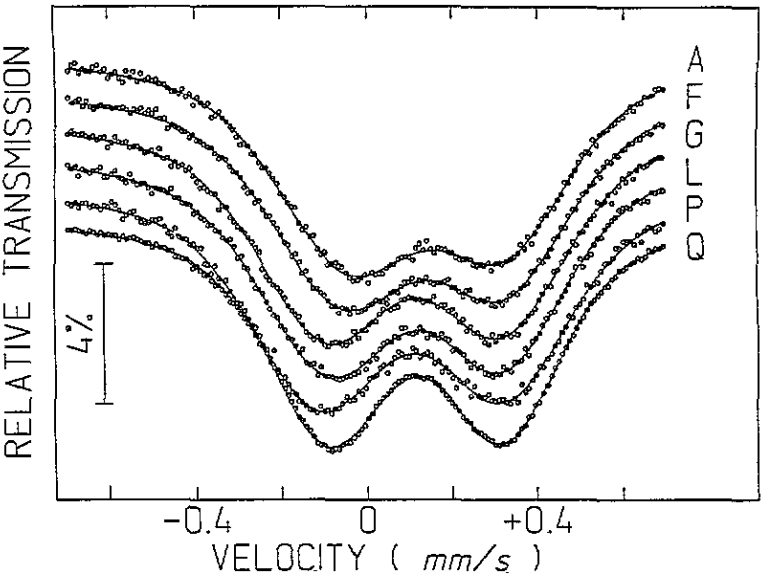

Figure 2. Mössbauer spectra (room temperature) showing a comparison between samples along the i-line (A, ico (24.4, 13) and F, ico (26.0, 12.2)) and along the r-line (the three samples G (ico), L (rhombo) and Q (penta), all at the same concentration (24.5, 11.9), and P, rhombo (28.0, 10.4)). All spectra are very similar with only small (but systematic) changes in the EFG splitting, central line shift and line broadening between the first two (A, F) and the last four (G, L, P and Q).

to a symmetrical broadening of the spectral lines, while the cross-correlation coefficient leads to an apparent line width asymmetry (with however equal line areas). In practice, we cannot separate the two contributions to the symmetrical line broadening, but we can separate the cross-correlation coefficient. The width of the combined distribution which we obtain can be considered as an upper limit to the real width of the Δ distribution. To obtain these coefficients, the spectra have been evaluated using a line profile of Voigt form including a full transmission integral formalism. The Voigt lineform is the convolution of a Gaussian (with standard deviation σ) and a Lorentzian (with full width at half maximum FWHM Γ). We use a very accurate pseudo-Voigt form in practice to increase computing speed [25]. We express the line asymmetry as the ratio of the Lorentzian FWHM Γ_2/Γ_1 between the rightmost line 2 and the leftmost line 1. This expresses the cross-correlation coefficient. This simple procedure leads to empirical coefficients which we can then use to systematically compare different samples and structures (varying both composition and long-range order) without imposing additional model dependence. In general, the quality of our fits yields values of χ^2 between 0.95 and 1.5. A feature of these evaluations is that we have assumed equal areas for the two quadrupole lines. Unequal areas have been often reported for different ico systems. A fit of our results using different areas for the upper and lower lines is also possible [21] but does not give a statistically significant improvement.

We have preferred here to represent the combined distribution with this Voigt-profile lineform, but do not claim that this is the exact one, only that it approximates it well enough for our purposes here. Alternatives for the distribution function include the χ^2 distribution for $n = 5$ degrees of freedom $P_5(\Delta) = \frac{1}{3}(2/\pi)^{1/2}(\Delta^4/s^5)\,e^{-(1/2)(\Delta/s)^2}$ which results from the Czjzek shell distribution [26], but has in fact been shown to be a much

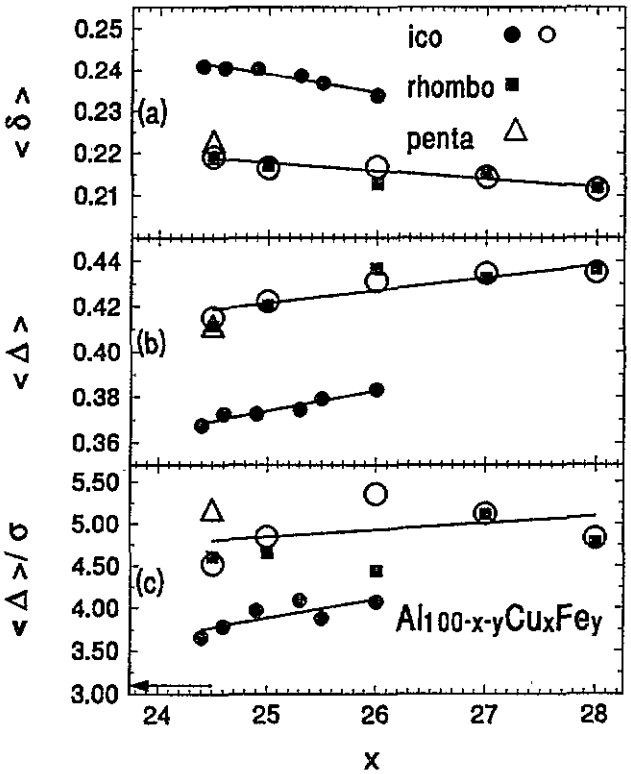

Figure 3. (a) Average ^{57}Fe central line shift $\langle\delta\rangle$, (b) average ^{57}Fe EFG splitting $\langle\Delta\rangle$, (c) ratio of the average quadrupole splitting to the standard deviation $\langle\Delta\rangle/\sigma$, as a function of the Cu concentration x. Data are taken from table 1. Solid circles represent LT stable ico alloys along the i-line (samples A–F). Open circles represent LT metastable ico alloys along the r-line (samples G–K). Solid boxes represent LT stable rhombo alloys (samples L–P). An open triangle represents the LT metastable pentagonal alloy (sample Q). The error bars are smaller than the symbol size. The solid lines are linear least-squares fits to the data for the ico samples along both i- and r-lines. Shown in (c) is an arrow indicating the GIM result (see text).

more general result [27]. Such a distribution for Δ can be obtained by assuming that the electric field gradient (EFG) tensor (**V**) components V_{ij} (not diagonalized) are independently distributed according to the same Gaussian law. For this reason, this distribution is better termed the Gaussian independent model (GIM) [27]. There is only one parameter s in the resulting distribution for Δ, so that the average value of Δ and the standard deviation of the distribution σ_Δ are related: $s = (9\pi/128)^{1/2}\langle\Delta\rangle = (9\pi/(45\pi - 128))^{1/2}\sigma_\Delta$. The above form for P_5 has been integrated over the anisotropy coefficient η. It is sufficient in the case of such distributions to take the average value: $\langle\eta\rangle \sim 0.61$ [27]. This distribution does not give as good results as the one presented above. The distribution assumed by Lawther and Dunlap [17] $P_n(\Delta) \propto (\Delta^{n-1}/s^n)\,e^{-(1/2)(\Delta/s)^2}$ with variable n is neither the shell distribution (as is often erroneously stated in the literature) nor is it clear where such a distribution could come from (see discussion in [27]). It is at best an empirical fit to data since it does not seem meaningful to make the degrees of freedom of the EFG tensor a variable. A further problem arises from the often-made assumption that there is a linear relationship between the quadrupole splitting and the central line shift. There is in general no reason to assume that any such relation exists (that is, one value of δ is related to one value of Δ). The more

reasonable assumption which we have made is that there is a correlation coefficient between the two distributions (although this is very small as given by the values of Γ_2/Γ_1 being very close to unity). Both distributions contribute to the experimentally determined value of σ. In the case of ^{57}Fe Mössbauer spectroscopy of non-magnetic samples, only in-field spectra allow separating (in principle) the two distributions. For spectra taken in zero field, we measure $\Delta \propto |V_{zz}|$, and not V_{zz} itself (V_{zz} is the largest eigenvalue of the EFG tensor). *Thus the contributions for the two signs of V_{zz} in the sample, but for possibly different* values of δ, are summed. This leads to a further apparent broadening for zero-field spectra.

3.2. Experimental results

The resulting parameters for Lorentzian FWHM Γ_1, line width asymmetry Γ_2/Γ_1, Gaussian standard deviation σ, average central line shift $\langle\delta\rangle$ and average quadrupole splitting $\langle\Delta\rangle$ are given in table 2, for the ico samples on the i-line (samples A–F), the metastable ico samples along the r-line (G–K) and the rhombo samples along the r-line (L–P), as well as one penta sample (Q) on the r-line. (The central line shift is reported with respect to BCC Fe at RT.) The samples studied here are relatively evenly distributed along the whole stability ranges which we have denoted as the i-line and the r-line. In addition to the hyperfine parameters for each sample given in table 2, the averages over the sample groups (A–F, etc) are also given, as they reflect the typical properties of each group. One further sample, R, has a composition which lies between the two lines. *The most striking result is the relatively constant values for $\langle\delta\rangle$ and $\langle\Delta\rangle$ for all the samples along the i-line or along the r-line, with a small but significant change going from the samples along the i-line to those along the r-line. There is essentially no difference between the ico samples along the r-line and their counterparts at the same composition in the rhombo state.* This is shown in figure 2 for the samples A and F as compared to L, G, Q and P. In table 2 we see an increase of about 0.023 mm s^{-1} in $\langle\delta\rangle$ for the ico samples from those on the r-line to those on the i-line (averaged over all samples on the respective lines), while there is essentially no change in $\langle\delta\rangle$ from the rhombo samples to the metastable ico samples along the r-line. Similar results are obtained for the values of $\langle\Delta\rangle$ averaged over the two lines, with a change of 0.053 mm s^{-1} between the two sets of ico samples and no change between the ico and rhombo samples along the same line. The penta sample shows a significantly smaller linewidth (see figure 2). These results are all presented in figure 3(a) for the central line shift and in figure 3(b) for the quadrupole splitting as a function of at.% Cu. Similar plots are obtained as a function of either iron or aluminum concentration (due to the linear substitution relations). The composition dependences of $\langle\delta\rangle$ and $\langle\Delta\rangle$ along the lines can be approximated by linear relations. We find for $\langle\delta\rangle$ a slope of about -0.0045 mm s^{-1} per % Cu (0.009 mm s^{-1} per % Fe), and along the r-line of about -0.0019 mm s^{-1} per % Cu (0.005 per % Fe). Notice that the change in $\langle\delta\rangle$ per % Cu is much faster away from than along either the perfect i-line or along the r-line. We must now consider the different contributions which might lead to the changes in the Mössbauer hyperfine parameters $\langle\delta\rangle$ and $\langle\Delta\rangle$ both along as well as between the two stability lines and between the different structures on the r-line. These include electronic effects but also possible changes in the lattice parameter (so called chemical pressure), and in the lattice vibrations. The measured central line shift at temperature T is given by $\delta(T) = \delta_{ch} + \delta_{SOD}(T)$. The chemical isomer shift δ_{ch} is proportional to the total s electron density at the nucleus $\delta_{ch} = \alpha\langle|\Psi_s(0)|^2\rangle$ with $\alpha < 0$ for ^{57}Fe. The second-order Doppler shift $\delta_{SOD}(T)$ depends on the lattice vibrations: $\delta_{SOD}(T) = -\langle v^2\rangle/2c$ where $\langle v^2\rangle$ is the mean square velocity of the Mössbauer nucleus and c is the velocity of light. We can estimate the possible effects by using the Debye model

Table 2. Results of the room temperature Mössbauer spectra: Γ_1 is the absorber Lorentzian line width of the leftmost line, Γ_2/Γ_1 the ratio of the widths of the rightmost to the leftmost line, σ the standard deviation of the Gaussian distribution (see text), $\langle\Delta\rangle$ the average EFG splitting, and $\langle\delta\rangle$ the average central line shift. For the letters used to label the samples, refer to table 1.

Sample	Γ_1 (mm s^{-1})	Γ_2/Γ_1	σ (mm s^{-1})	$\langle\Delta\rangle$ (mm s^{-1})	$\langle\delta\rangle$ (mm s^{-1})
A	0.1440	1.1303	0.1005	0.3675	0.2409
B	0.1629	1.0791	0.0985	0.3723	0.2404
C	0.1565	1.0945	0.0939	0.3724	0.2402
D	0.1620	1.0870	0.0916	0.3744	0.2385
E	0.1485	1.1107	0.0978	0.3791	0.2367
F	0.1549	1.0761	0.0941	0.3831	0.2337
Average A–F	0.1548	1.0963	0.0961	0.3748	0.2384
G	0.1545	1.0682	0.0918	0.4150	0.2191
H	0.1099	1.1118	0.0872	0.4221	0.2164
I	0.1186	1.0655	0.0805	0.4310	0.2167
J	0.1053	1.1443	0.0849	0.4346	0.2143
K	0.1439	1.1048	0.0901	0.4349	0.2114
Average G–K	0.1264	1.0989	0.0869	0.4275	0.2156
L	0.1582	1.0500	0.0893	0.4114	0.2188
M	0.1579	1.0682	0.0903	0.4201	0.2170
N	0.1503	1	0.0984	0.4365	0.2127
O	0.1651	1.0518	0.0846	0.4324	0.2151
P	0.1505	1.1127	0.0913	0.4363	0.2118
Average L–P	0.1564	1.0565	0.0908	0.4273	0.2151
Q	0.1290	1.0422	0.0796	0.4117	0.2228
R	0.1610	1.0861	0.0969	0.3964	0.2300

(see Shenoy in [28], p 108), where δ_{SOD} is calculated from the Debye temperature Θ_D. The variation in δ_{SOD} with changes in Θ_D can be expressed in the high-temperature limit as $\Delta\delta_{SOD} \sim \frac{4}{15}\delta_{SOD}(0)\,\Delta\Theta_D/T$. The parameter $\delta_{SOD}(0)$ is the zero-point second-order Doppler shift given by $\delta_{SOD}(0) = -9k_B\Theta_D/16Mc$, where k_B is the Boltzmann constant and M is the atomic mass (of ^{57}Fe). From our low-temperature measurements (to be published) reasonable values are $\delta_{SOD}(0) \sim 0.1$ mm s^{-1} and $\Theta_D \sim 500$ K. If the changes in the measured $\langle\delta\rangle$ at room temperature were ascribed to Θ_D variations, they would lead to changes in Θ_D of about 80 K along the i- and r-lines, and at least 220 K between them. For such small changes in composition, these variations seem to be too large to be physically acceptable. We now estimate possible changes in the central line shift due to the observed changes in the 6D lattice constant given in table 1, considering these to result in a chemical pressure on the iron atoms. It is usual in pressure studies to report the empirical pressure dependence of the central line shift as $\mathrm{d}\,\delta(T)/\mathrm{d}\,\ln V$, where V is the volume (see Williamson in [28], p 332). This coefficient includes a combination of several factors in addition to the simple variation of the electron density with decreasing volume. Typical values of this parameter are in the range of 0.8–1.2 mm s^{-1} for ^{57}Fe in simple light-metallic matrices, and up to 1.8 mm s^{-1} for some matrices with large atomic numbers. In order to explain our variations in the central line shift along the i- and r-lines we would have to assume a value of at least 2 mm s^{-1}, which is too large to be physically acceptable. We conclude that such chemical pressure changes might be present, but could in any event only account for a maximum of about 50% of the variations along the two lines. The variation

between the two lines cannot be explained by this variation because it is possible to choose different compositions (say x_1 on the i-line and x_2 on the r-line) with the same value of a_{6D}. These results show that *there is no change in the total s electron density between the ico and approximant structures at constant composition, but there is an increase going from the stable ico (along the i-line) to the metastable ico or stable rhombo (along the r-line).* Let us recall that there is also essentially no change in the average quadrupole effect $\langle\Delta\rangle$ going from the ico to approximant structures at constant composition but a increase of about 0.053 mm s^{-1} from the i- to the r-lines. The remaining variation of $\langle\Delta\rangle$ with composition along each line is small. The volume dependence of the electric field gradient is generally reported as $d\ln V_{zz}/d\ln V = -K$ where a point charge model gives $K = 1$, but typical experimental values are generally in the range of 2–5 [29]. In order to explain the slow variation of $\langle\Delta\rangle$ along the two stability lines as simply a volume dependence (chemical pressure), then we would need $K \sim 16$, a value which is much too large to be physically acceptable. We then must conclude that the slow variation of both $\langle\delta\rangle$ and $\langle\Delta\rangle$ along the stability domains cannot be entirely attributed to volume effects, or to changes in the Debye temperature. This variation must therefore reflect small residual changes in the electronic properties, much smaller than those observed between the two lines.

Shown in figure 3(c) is the ratio $\langle\Delta\rangle/\sigma$ for our samples as a function of Cu concentration. We note in passing that the values of Γ obtained from the fits (table 2) are close to the natural absorber line width $\Gamma_0 \sim 0.19$ mm s^{-1}, so that σ provides a reliable estimation of the distribution width. We use σ as an upper bound for σ_Δ. Also shown by an arrow in figure 3(c) is the GIM result $\langle\Delta\rangle \sim 3.094\,\sigma_\Delta$. The large deviations observed in our samples from this model result clearly show that in fact the sample spectra are not adequately described by this model. Smaller values of σ_Δ would only increase this discrepancy. The GIM distribution describes a completely *random* EFG distribution, and was first postulated for non-magnetic amorphous alloys. But all samples studied here show very well defined (quasi-) crystalline order as shown by the x-ray results. It is also significant that the results for the ico samples along the i-line are at smaller $\langle\Delta\rangle/\sigma$ values than the ico and rhombo samples along the r-line. These results will be discussed further in section 5, together with those from NMR.

4. ^{27}Al NMR data

4.1. Spectra

The ^{27}Al spin echo was measured in a fixed external magnetic field $B_0 = 6.996$ T, at room temperature on the same samples as used in the Mössbauer studies. A sequence of two coherent RF pulses, $\pi/2$ (duration 7 μs) and π (14 μs), separated by a time $\tau = 100$ μs, was used to generate the spin echo. A typical spectrum is shown in figure 4 for sample E. Similar spectra are observed in all the samples studied. It consists of a narrow central line associated with the $m = -\frac{1}{2}$, $m = +\frac{1}{2}$ nuclear spin transition, superimposed on a broad line with a width of about 5 MHz due to the quadrupole splitting on the remaining four nuclear transitions of the Al nucleus ($I = 5/2$), as previously reported [6, 18, 23]. The absence of any resolved quadrupolar satellite indicates a broad distribution of local environments at the Al site. Similar ^{27}Al NMR spectra have been observed in other QC alloys such as AlMn, AlLiCu, AlPdMn [6, 30]. No other phases could be found in these NMR spectra, confirming the Mössbauer and x-ray studies. We will focus in the following on the properties of the narrow central line as represented in figures 5 and 6. The Hamiltonian describing the Al NMR in a metallic sample can be written as $H = H_Z + H_C + H_D + H_Q$. The first term is

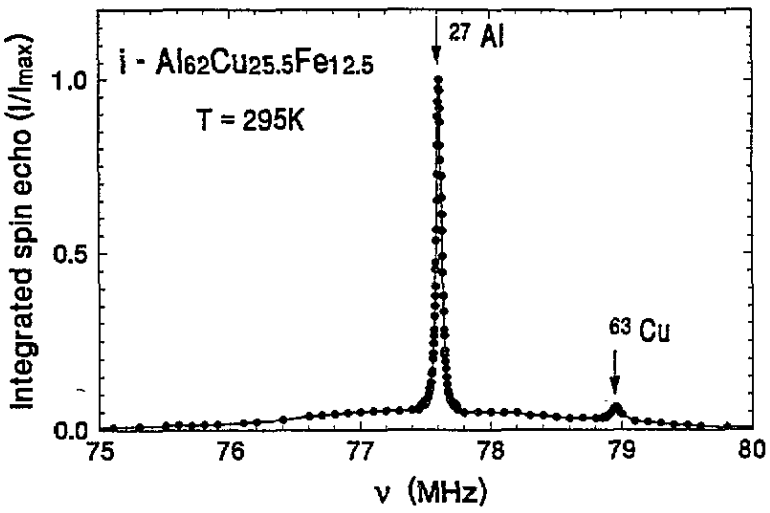

Figure 4. Typical NMR spectrum (integrated spin echo) obtained by sweeping the frequency in a fixed field $B_0 = 6.996$ T. Arrows indicate the reference positions for the ^{27}Al and ^{63}Cu resonances. The intensity has been normalized to the maximum value. The RF pulse lengths were fixed in order to maximize the ^{27}Al signal. The ^{63}Cu signal is then strongly reduced. The curve shown is only meant as a guide for the eye.

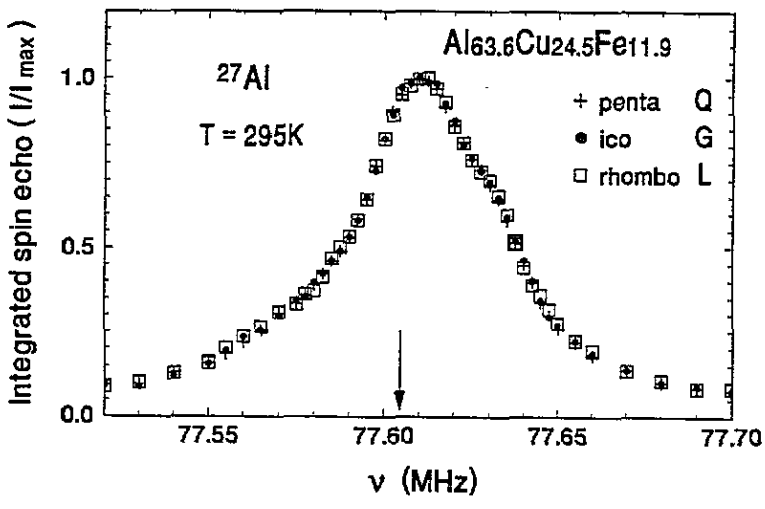

Figure 5. Comparison of the ^{27}Al NMR lines ($m = \frac{1}{2}$, $m = -\frac{1}{2}$ nuclear transition only) of three of the samples as in figure 2: L (rhombo), G (ico) and Q (penta). No difference in the shape or the position of the ^{27}Al NMR line is detected. The arrow indicates the reference position ($\nu_0 = 77.6047$ MHz).

the nuclear Zeeman effect of the spin I in an external field B_0 given by $H_Z = -\gamma_n \hbar I \cdot B_0$. The second term is the contact interaction of the nuclear spin with the conduction electrons. The third term is the dipolar interaction between the nuclear and electron spins. The fourth term is the quadrupolar interaction of the nucleus with the local electric field gradient (as before for the Mössbauer effect). When H_Q is zero (for nuclei in cubic or higher symmetry)

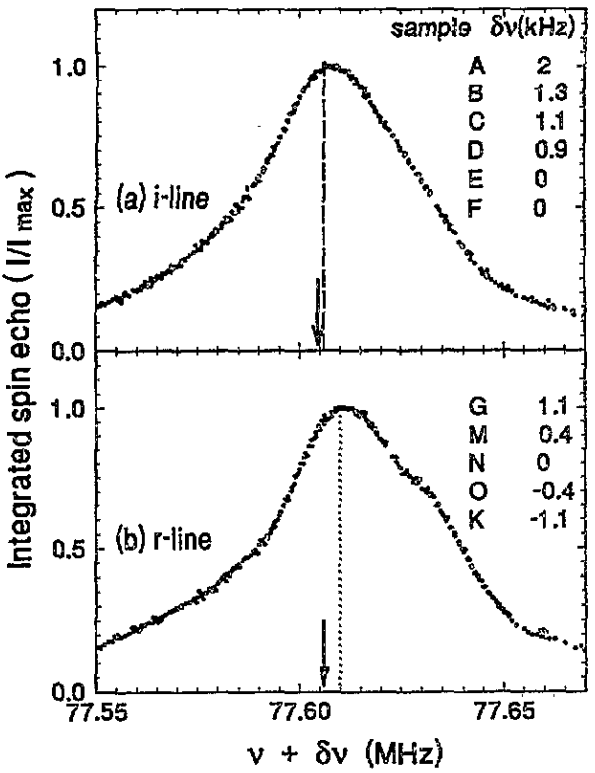

Figure 6. Comparison of the ^{27}Al NMR lines ($m = \frac{1}{2}$, $m = -\frac{1}{2}$ nuclear transition only) measured in the stable icosahedral samples (a) along the i-line and (b) in ico and rhombo samples belonging to the r-line. In (a) and (b), the spectra have been translated by $\delta\nu$ (indicated on the figure) chosen to achieve the best possible superposition with the spectrum of sample E for (a) and N for (b). Along each line all the spectra merge on a single curve, which demonstrates that the line shape of the ^{27}Al resonance is the same for all samples along one line, but differs between them. The arrows indicate the reference position as in figure 5, while the lines indicate the average position of the line (sample E for (a) and N for (b)).

the resonance occurs at $\nu_r = \nu_0\ (1 + K_s)$, where $\nu_0 = \gamma_n B_0$, is the reference frequency of bare ^{27}Al nuclei in the external applied field B_0, and the *positive* term K_s is the Knight shift, due to the contact interaction between the nucleus and the s part of the conduction electron wave function. $K_s = (8\pi/3)\langle|\Psi(0)^2|\rangle_{FS}\chi_p$, where $\chi_p = \mu_B^2 N(E_F)$ is the Pauli susceptibility of the electron gas per atom, and $\langle|\Psi(0)^2|\rangle_{FS}$ is the density of s electrons at the nucleus averaged over the Fermi surface. The H_D term of the Hamiltonian does not shift the resonance in a powder sample but leads to a broadening of the NMR line. Note that an eventual distribution of the K_s values will also affect the line width. H_Q affects the $m = \frac{1}{2}, m = -\frac{1}{2}$ nuclear transition to second order in perturbation. In a powdered material, this leads to a broadening of the line and to a *negative* shift. Then the average frequency of the line $\langle\nu\rangle$ is smaller than ν_r, the difference $\langle\nu\rangle - \nu_r$ being proportional to the quadrupolar broadening. No magnetic broadening (as observed for example in QC $Al_{80}Mn_{20}$ [31]) is expected at room temperature in the AlCuFe quasicrystals, in view of their small susceptibility [22].

A fit of the NMR line is required to determine ν_r, which implies making a hypothesis

on the distribution of the electric field gradient parameters and separating the different contributions to the total line width. This is impossible in the absence of additional experimental information. Therefore in the next section we will only perform qualitative comparisons of the Al NMR lines observed in the different samples and use $\langle\nu\rangle$ to estimate the line position. A more quantitative analysis will be attempted in section 4.3.

4.2. Line shape and line position

In order to detect the possible influence of the nature of the long-range order on the parameters of the ^{27}Al NMR line, we have systematically compared results for the icosahedral and the rhombohedral states for compositions along the r-line. For the composition $Al_{63.6}Cu_{24.5}Fe_{11.9}$ we also measured the pentagonal state, as illustrated in figure 5. *At a given composition no difference exists between the ^{27}Al NMR line observed in the approximant and icosahedral states.* On the other hand *clear changes of both the line position and the line shape are observed when comparing samples with different compositions,* as illustrated in figure 6. In the following we shall use interchangeably the ico or approximant state at a given composition as NMR spectra can make no distinction between these two states.

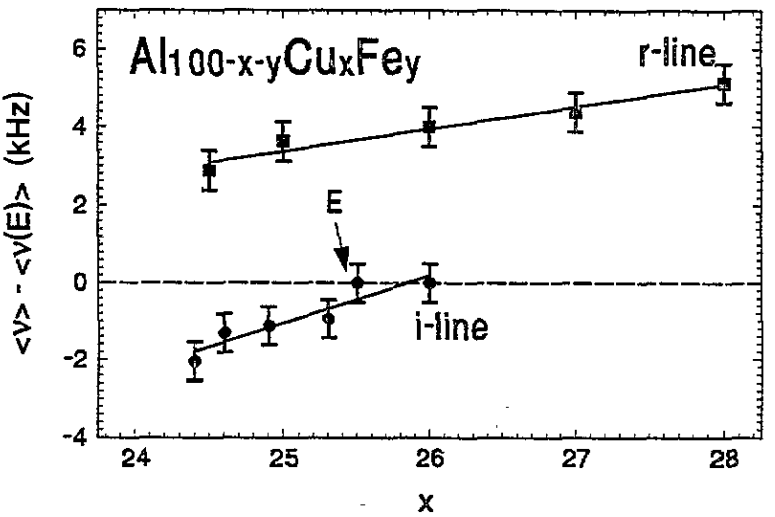

Figure 7. Average frequency $\langle\nu\rangle - \langle\nu(E)\rangle$ of the ^{27}Al NMR central line for the ico samples on the i-line, and for the rhombo samples on the r-line, referred to that of sample E ($\langle\nu(E)\rangle$). The lines are linear least-squares fits to the data along the i- and r-lines.

Systematic trends appear when we compare all the samples studied here. First the NMR line for any sample along the i-line occurs at a lower frequency than the NMR line of any sample along the r-line. Second, *the ^{27}Al NMR line shapes of all icosahedral samples along the i-line are identical. Only small position changes occur.* This is illustrated in figure 6(a) where the resonance lines of the six icosahedral samples along the i-line (A–F) have been superimposed to a very good accuracy on the curve for sample E, by simply translating the curves by a small, sample-dependent, amount $\delta\nu$. The maximum translation, from sample A to sample F, at the two ends of the i-line, is ~2 kHz. We emphasize that a positive $\delta\nu$ value corresponds to a NMR line occurring at a smaller frequency than the line of sample E. We have therefore reported in figure 7 $-\delta\nu$ as a function of the Cu concentration x, which is equivalent to plotting the average frequency of the NMR line versus x, setting $\langle\nu\rangle = 0$ for

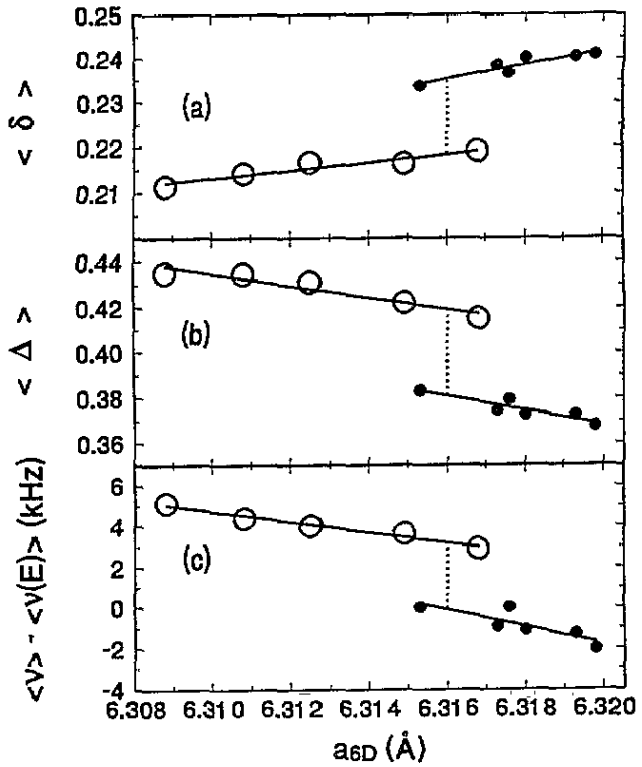

Figure 8. (*a*) ^{57}Fe *average line shift* $\langle\delta\rangle$, (*b*) ^{57}Fe *average quadrupole splitting* $\langle\Delta\rangle$ *and* (*c*) ^{27}Al average frequency $\langle\nu\rangle - \langle\nu(E)\rangle$ as a function of the 6D lattice parameter a_{6D}. The dotted lines connect values at $a_{6D} = 6.316$ Å. Solid circles represent LT stable ico alloys along the i-line, and open circles represent LT metastable ico alloys along the r-line. The lines are least-squares fits to the data.

sample E. $\langle\nu\rangle$ shows a small and continuous increase when the Cu concentration increases (~1.25 kHz/% Cu). A similar analysis can be performed for samples along the r-line (figure 6(b)) by comparing all samples with sample N. Here again *the* ^{27}*Al NMR line shapes of all samples along the r-line are identical. Only small position changes occur.* Surprisingly the line shape of the ^{27}Al NMR line for samples on the r-line slightly *differs* from that observed for samples along the i-line. Along the r-line the maximum translation, from sample G (or L) to sample K (or P), at the two ends of the r-line, is ~2.2 kHz and $-\delta\nu$ increases continuously with the Cu concentration, with a smaller slope ~0.6 kHz/% Cu than along the i-line. A plot of the $-\delta\nu$ values used to draw figure 6(b) as a function of the Cu concentration would be equivalent to a plot of $\langle\nu\rangle$ versus x, with $\langle\nu\rangle = 0$ for sample N. Then to compare these $-\delta\nu$ values with those obtained for samples along the i-line, we must add a constant value to them to account for the difference between the resonance positions in samples E and N. In figure 7 we have assumed this constant to be 4 kHz assuming $\langle\nu\rangle = 77.610$ MHz for sample N and $\langle\nu\rangle = 77.606$ MHz for sample E. It should be emphasized that the small line shape change between these two samples has only minor consequences on this value. Using another criterion to determine the line position, for example the frequency of the line maximum, leads to the same value within 10%. This means that in figure 7 an overall small vertical shift of all the data for the r-line with respect to the data for the i-line, not included

in the error bars, is allowed. This small uncertainty does not affect the fact, observed on raw spectra, that the average frequency $\langle\nu\rangle$ of the ^{27}Al NMR line of any sample along the i-line is smaller than that of any sample along the r-line.

4.3. Analysis

In summary one can decompose the change in the Al NMR from the i-line to the r-line into an overall shift of the resonance line towards higher frequencies accompanied by a very small change of the shape. Along each line the shape is constant and only small position changes occur. To analyse these NMR results more quantitatively, one needs to identify the main contributions to the line width and shift.

A first question is whether the changes in the NMR line frequency from sample to sample reflect changes in the electronic structure, via the contact interaction, or whether they could result from changes in the quadrupolar couplings H_Q. Changes in H_Q affect both the line position and the width. Therefore for samples along a given line, i- or r-line, the small frequency changes occurring at constant line shape cannot be due to changes in H_Q. From the i-line to the r-line, as the line shape changes slightly, the answer is not so straightforward. To determine which part of the total line width (~45 kHz for the full width at half maximum) is due to H_Q, we measured the NMR spectrum of one sample (E) in a lower field ~1.2 T. (This spectrum was recorded by sweeping the applied field B_0 in a fixed frequency 13.4 MHz at 4.2 K.) In 1.2 T, the second-order quadrupolar splitting, which is proportional to B_0^{-1}, provides the dominant contribution to the line width of the central line. From the measured line width in 1.2 T (FWHM ~ 170 kHz), we estimate that the quadrupolar contribution to the line width is ~30 kHz in 7 T. The negative shift of the NMR central line induced by the quadrupolar couplings, $\langle\nu\rangle - \nu_r$, is proportional to the quadrupolar line width. Although the proportionality coefficient is not accurately known (as long as a theoretical spectrum is not calculated in a given model of the local environment distribution), we can safely assume that $|\langle\nu\rangle - \nu_r|$ is a small fraction of the quadrupolar line width and therefore does not exceed a few kHz in 7 T. Should the typical increase of the resonance frequencies from the i-line to the r-line (~4 kHz from sample E to sample N for example) be ascribed to changes in the quadrupolar couplings, it would then be accompanied by a clear decrease of the line width which is not observed. We can therefore conclude that *the observed changes of the NMR line positions from the i-line to the r-line are not due to changes in the quadrupolar coupling. They must then reflect a change in electronic structure* affecting all Al sites in a similar manner (neglecting for the moment the small change in line shape also found).

In all samples studied $\langle\nu\rangle$ is found very close to the reference frequency $\nu_0 = 77.6047$ MHz (the minimum value is 77.604 MHz in sample A and the maximum value is 77.611 MHz in samples K and P). The relative frequency shift $(\langle\nu\rangle - \nu_0)/\nu_0$ therefore never exceeds 0.08×10^{-3}. Similar observations were made previously in ico $Al_{62}Cu_{25.5}Fe_{12.5}$ [6], $Al_{63}Cu_{24.5}Fe_{12.5}$ [23] and $Al_{65}Cu_{23}Fe_{12}$ [18]. $(\nu_r - \nu_0)/\nu_0$ should be actually computed to obtain the electronic contribution to the line shift, in the absence of quadrupolar effects. As the difference $|\langle\nu\rangle - \nu_r|$ remains small, ~ a few kHz, we can assert that $(\nu_r - \nu_0)/\nu_0$ is also a very small quantity in all samples studied. For comparison, in metallic FCC Al, in the field used here, the resonance would occur at $\nu_r = 77.732$ MHz which is off scale on figures 5 and 6. ($\nu_0 = 77.6047$ MHz is actually calculated from the observed resonance in FCC Al, using the known Knight shift value $K_s = 1.64 \times 10^{-3}$ [32].) Therefore the main conclusion is that the isotropic Knight shift K_s is abnormally small in AlCuFe quasicrystals and approximants, compared to simple metals with mainly s character at the Fermi level.

Unfortunately going further is very difficult. Due to the smallness of K_s the Hamiltonian presented in section 4.1 may be no longer valid. In particular the chemical shifts have probably the same order of magnitude as the shifts due to the conduction electrons. Also, if the conduction electrons at the Fermi level have a p or d character at the Al site, the core polarization mechanism should be considered. Finally the validity of the usual expression for K_s should also be affected by the very anomalous Fermi surface expected in AlCuFe quasicrystals and approximants [33] and by the possible existence of critical states and the spiky nature of the density of states [34].

A pending question is the origin of the small change in the line shape of the ^{27}Al resonances between samples along the i- and the r-lines. One can calculate a difference spectrum by comparing the NMR line measured in sample N with that observed in sample E, shifted towards higher frequency by 4 kHz (to account for the difference of the average NMR frequencies in the two samples). Its area does not exceed $\sim$ a few % of the integrated spectrum of sample E or N. It is of course impossible to decide whether the change in the NMR spectrum results from a modification of the quadrupolar Hamiltonian, or from modifications of the local electronic properties, or more likely from both. All these results will be discussed with respect to the Mössbauer studies in the next section.

5. Discussion

When considering the hyperfine results obtained by Mössbauer and by NMR spectroscopy together, the following coherent picture emerges. First of all, no differences were detected for samples along the r-line having the same composition, but having different long-range order, periodic approximant or quasiperiodic. (The only exception to this was the small narrowing of the ^{57}Fe EFG distribution in the pentagonal alloy. However this effect would need further confirmation in other samples). This means that the local atomic environments and local electronic structure, on Al and Fe, are insensitive to the nature of the long-range order. This was also concluded in earlier EXAFS experiments [35], for the Fe and Cu sites. The similarity of the local environments found in the quasicrystals and the approximants is in agreement with current models in which both are built from the same large structural units [1]. We note however that in the EXAFS study [35], the comparison was made between a rhombo sample and an ico sample with a different composition, not along the r-line. The change which we have observed here between samples with different compositions seem therefore undetectable in EXAFS.

Focusing now on the concentration dependence of the different hyperfine parameters, we notice that the most striking result is the relatively large changes on going from the i- to the r-line. This includes the ^{57}Fe average central line shift $\langle\delta\rangle$ and average EFG splitting $\langle\Delta\rangle$, as well as the ^{27}Al average frequency $\langle\nu\rangle$ and associated NMR line shape. On the other hand, along either of the lines, there are only weak continuous variations of $\langle\delta\rangle$, $\langle\Delta\rangle$ and $\langle\nu\rangle$, and no change in the NMR line shape. In figures 3 and 7 these parameters were given as a function of the Cu concentration x. Similar results are obtained for the same parameters as a function of Al $(100 - x - y)$ or Fe (y) concentrations as the stability domains are practically lines. This results in linear relations between the concentrations.

We remark that these observations are striking because the composition changes involved going from one line to the other are actually smaller than those involved between the two limiting compositions along one line. For example, at constant x, going from the i- to the r-line involves a change of 1.1% of the Al atoms being replaced by Fe atoms. But along the r-line, there is a change of 3.5% of the Al atoms. These are replaced along the line according to the following rule: 1 Al atom and 0.66 Fe atoms are replaced by 1.66 Cu

atoms. We conclude that the changes in the hyperfine properties scaled by the percentage change in composition are much larger between the two stability domains than along them. The nature of the substitution is therefore critical.

Let us first focus on the changes *between these two lines*, neglecting for the moment the small changes along them. *The electronic structure clearly changes* in this transition, despite the relatively small composition change. This change affects all the Fe and Al atoms and not just some of them since we see shifts of the NMR line and Mössbauer spectra with reasonably constant line width (neglecting the very small change of the NMR line shape). On going from the i- to the r-line, $\langle\delta\rangle$ decreases, showing that there is an increase in the local density of s electrons at the Fe site, as has been discussed above. The increase in $\langle\nu\rangle$ is more difficult to interpret since the contribution due to the isotropic Knight shift K_s cannot yet be separated from other contributions, as has been explained in section 3.3. These changes in electronic structure between the two lines are associated with changes in the distribution of local electrical field gradients. In the case of the Fe sites, this is very clear as the ^{57}Fe $\langle\Delta\rangle$ unambiguously increases (i- to r-line). The parallel small change in the ^{27}Al line shape also reveals a modification of the local environments although we do not know to what extent these are EFG or electronic changes.

A simple explanation of the changes in the local EFG on the Fe sites would be the following. At constant Cu concentration, ~10% of the Fe atoms are replaced by Al atoms when we go from the i- to the r-line. As a very crude model we can assume that the loss of iron atoms leads to a loss of certain environments, namely those with a smaller value of Δ. It is very difficult to reconcile this with the fact that along either the i- or the r-line, substituting ~10% of the Fe atoms does not lead to comparable changes in Δ. The only way to reconcile these two different sensitivities to changing Fe composition is to assume that they involve different substitutions. The variation of the hyperfine parameters along one line is similar to that in a solid solution, so that there is a random substitution. From one line to the other, either there is a structural change inducing large changes in properties, or the substitution is not isomorphous and involves only a certain category of sites.

Finally we should re-emphasize here that although changes in a_{6D} occur from the i-line to the r-line, they cannot be the reason for the differences in the hyperfine properties observed since in fact *compositions exist on the two lines with the same value of a_{6D} but having different properties*. In figure 8, we show the variation in the ^{57}Fe Mössbauer parameters $\langle\delta\rangle$ and $\langle\Delta\rangle$ and the ^{27}Al NMR parameter $\langle\nu\rangle$ as a function of a_{6D}. The dotted lines connect the i-line and the r-line values at a constant value of $a_{6D} = 6.316$Å, the same as that which was given in figure 1.

Relative to the changes observed between the i-line and the r-line, the slow variation of $\langle\delta\rangle$, $\langle\Delta\rangle$ and $\langle\nu\rangle$ within them indicates that the electronic structure is here practically constant. As explained in section 3.2 these slow variations in $\langle\delta\rangle$ and $\langle\Delta\rangle$ cannot be entirely ascribed either to the continuous change of the 6D lattice parameter a_{6D}, or to possible changes in the Debye temperature, although they may partially contribute. A quantitative analysis of the variation of $\langle\nu\rangle$ with changes in a_{6D} is not possible as long as the origin of the line shift is not better understood, but (chemical) pressure effects if they are present will naturally also affect K_s [32]. Changes in the Debye temperature would of course have no effect on $\langle\nu\rangle$.

Then the main conclusion of this work is *the relative insensitivity of the electronic structure for composition changes within one domain, and the much larger changes between them, although the composition change can be much more important in the first case.* In the framework of Hume-Rothery arguments, widely used in the literature to explain the pseudogap formation in quasicrystals and high-order approximants [3, 10, 33], this finding

has a very natural explanation, as has been mentioned in the introduction. We shall now develop this idea further although it implies making very crude approximations which may well not be fully justified, especially in alloys with transition metals. In a free-electron picture, one can write the condition for the pseudogap formation as $k_F \sim Q/2$, where Q is the average norm of the reciprocal lattice vectors of the pseudo-Brillouin zone (PBZ) defined from the strongest x-ray diffraction spots. This leads to the well known Hume-Rothery criterion on the average number of conduction electrons per atom, e/a, as $k_F = (3n\pi^2)^{1/3}$ where the electron density n is given by $n = (e/a)\rho N_A/M_A$. In this expression ρ is the density, N_A is the Avogadro number and M_A the atomic mass. The density of a quasicrystal is a parameter which is very difficult to measure accurately. In the following discussion we have used a constant value $\rho = 4.40$ g cm^{-3} for all samples (measured on an $Al_{63}Cu_{25}Fe_{12}$ ico sample in a bulk form). The value of e/a is given by a weighted sum of the conduction electrons per atom (effective valencies) over the different atomic species. Here, $e/a = (100-x-y)v_{Al} + xv_{Cu} + yv_{Fe}$. The usual choices of $v_{Al} = 3$, $v_{Cu} = 1$ are quite reasonable. The main problem here, as in most cases of Hume-Rothery alloys containing transition metals, is to decide on the appropriate valence for Fe (or other transition metal). An empirical *negative* valence has often been used in the literature [36]. This is not to be thought of as a real valence, and indeed a hypothetical Fe^{2-} would give a $\langle\delta\rangle$ vastly different than that observed here (typical for Fe in Al alloys). Recently an explanation was proposed to justify taking negative valencies for transition metals [37] due to the d states close to the Fermi level.

The stability lines in the phase diagram can be interpreted as isoelectronic lines, i.e. lines at constant e/a. The observed slopes are consistent with $v_{Fe} = -2$. Then $e/a = 1.865$ for the samples along the i-line and $e/a = 1.92$ for the samples along the r-line. These are the solid lines given in figure 1. Values of v_{Fe} between -2.5 and -1.5 would also lead to the same conclusion, with only slight changes in the slopes given in figure 1. Calculating k_F using the expression given above, we find for *all* samples values which match the diameter of the PBZ as built from the (0/0 0/0 2/4) Bragg peak ($Q = 19.79/a_{6D}$) and (0/0 1/2 2/3) Bragg peak ($Q = 18.82/a_{6D}$). The usual Hume-Rothery condition ($k_F \sim Q/2$) is therefore not accurate enough to justify the existence of two distinct stability lines with close values of e/a. This is not surprising as the above criterion only takes into account the variation of the Fermi energy at constant band structure in a free-electron picture. Improvements in this prediction would require more detailed knowledge of the Fermi surface and an accurate treatment of the d states of the iron.

Our results are coherent with the Hume-Rothery model of the phase stability in the sense that only minor changes in the electronic structure are observed within each domain. The question now arises of whether we can change e/a by taking other paths on the phase diagram, and studying the associated changes in hyperfine parameters. One such choice would be a path perpendicular to the two lines of constant e/a studied here. Unfortunately this turns out to be very difficult in the case of the AlCuFe phase diagram. If we try to go to a lower e/a value than that of the i-line or to a larger value than that of the r-line, this leads to a two-phased region of the phase diagram. Although these observations reinforce the importance of the e/a ratio to stabilize a QC or approximant phase in AlCuFe, the consequence is that we are strongly limited in allowed variations. The only meaningful additional study would be at compositions between the two lines, for example for sample R given in table 1 ($e/a = 1.885$ using $v_{Fe} = -2$). The values for $\langle\delta\rangle$, $\langle\Delta\rangle$ (see table 2) and $\langle\nu\rangle$ (= 77.6075 MHz) for this sample are intermediate between those for the i- and the r-line, and even the NMR line shape is intermediate between that given in figure 6(a) (i-line) and figure 6(b) (r-line).

Finally it is interesting to compare the present results with those available in the literature on the compositional dependence of electronic properties of QC and approximant systems. Most of these studies have been performed on metastable QC alloys. One of the more complete is that of Wagner *et al* on AlCuMg and GaZnMg [38] who observed anomalies in the evolution of the electronic properties as a function of composition and ascribed this to a deepening of the pseudogap at the composition corresponding to the best matching between the Fermi surface and the PBZ. No correlation with stability could be made as all these alloys are metastable.

Dunlap [39] has presented ^{57}Fe Mössbauer results for the $Al_{75}Fe_{25-x}Ni_x$ decagonal phases as a function of e/a. In the composition range $x = 3$–16, he found variations in $\langle\delta\rangle$ and $\langle\Delta\rangle$ which are large compared to those presented here. Rather than the linear variation which we have found, $\langle\delta\rangle$ presents a clear maximum near $x = 9$, while $\langle\Delta\rangle$ shows a non-linear but monotonic increase with x. He analysed his results in a Hume-Rothery model in order to show that this maximum in $\langle\delta\rangle$ represents a point of maximum stability due to a gap formation at the Fermi surface (and so decreasing $\langle|\Psi_s(0)|^2\rangle$). He has calculated the values of Q for the decagonal PBZ for the different samples, and compared them to the values of $2k_F$ as calculated in a free-electron picture. His conclusion is that the maximum in $\langle\delta\rangle$ represents the point where $2k_F = Q$. However, this result strongly depends on the exact choice made for the Fe valence v_{Fe}, which he took as -2.66 from [36]. Another choice of v_{Fe}, for example -2, would completely remove this agreement. In addition a strong variation of Q is observed among the samples studied here. The lattice parameter indeed goes through a minimum for $x = 9$. No correction of $\langle\delta\rangle$ for these volume changes is made in [39]. Making this correction would reduce the maximum in $\langle\delta\rangle$. Thus we conclude that the conclusions made in [39] are questionable. In addition, the idea of a peculiar stability of the decagonal $Al_{75}Fe_{16}Ni_9$ phase is not supported by the recent investigations of the AlFeNi phase diagram by Lemmerz *et al* [40], the decagonal phase being stable in a narrow composition range around $Al_{71}Fe_{24}Ni_5$.

In stable QC alloys only a few results are known. Systematic studies of the transport properties of AlCuFe QC and rhombohedral approximants have been performed. A perfect identity is found between the ico and rhombo phases at the same composition [2]. Lindqvist *et al* [41] have studied 20 different ico samples and shown that the low-temperature conductivity $\sigma(4\ \mathrm{K})$ does vary with composition. However, its variation versus e/a (assuming $v_{Fe} = -2$) only shows a very erratic behaviour. Changing the Fe valence from the -2 value does not lead to any improvement. On the other hand, $\sigma(4\ \mathrm{K})$ displays a clear dependence on the Fe concentration, with a minimum near 12.5% Fe. The Hall coefficient at 4.2 K is also correlated to the Fe concentration. It seems therefore that the transport properties are not very sensitive to the value of e/a, but rather strongly influenced by the Fe d states. Pierce *et al* [7] have presented the low-temperature electrical conductivity and specific heat of four AlCuFe samples. They observed a change in $\sigma(4\ \mathrm{K})$ between the ico and rhombo phases at the same composition which was not observed in [2], and also a suprising change in γ as well.

6. Conclusion

We present here the first study of the local electronic properties and local order *along the stability lines of an icosahedral quasicrystal and approximant systems*. We have shown that the electronic properties and the local environments are insensitive to the long-range order (quasicrystalline or crystalline approximant), but sensitive to the changes in average number of conduction electrons per atom, e/a. The similarity found between the QC AlCuFe and

its rhombohedral approximant, which is a high-order approximant (3/2), is not surprising as both of these structures are built up from the same large building blocks. The electronic properties which are important here, namely the pseudogap in the density of states, are present in all but the lowest-order approximant structures [8]. We have shown that the two isostructural stability lines in the AlCuFe phase diagram, denoted here as the i-line and the r-line, are nearly isoelectronic. Our results therefore demonstrate the importance of the type of chemical substitution. From the variation of the 6D lattice parameter a_{6D} with composition it is possible to produce samples with the same value of a_{6D} but belonging to different stability domains. These show different local electronic properties and also have slightly different local order. These observations have a very natural explanation within the Hume-Rothery scheme of phase stability. We have observed here slow variations of the electronic properties along the stability lines and larger ones between them. More information relating to the electronic properties at the Fermi level would be very useful to support our conclusions. In principle, specific heat data give direct information on the density of states at E_F, but such results are often difficult to interpret if traces of magnetic phases are present. These can vary erratically from sample to sample and can easily mask the expected small variations in the electronic term γ with composition. There are unfortunately not enough results in the literature to allow us to determine the compositional dependence of γ.

Acknowledgment

We would like to thank D Gratias (CECM, Vitry) for fruitful discussions.

References

[1] Goldman A I and Kelton K F 1993 *Rev. Mod. Phys.* **65** 213
[2] Mayou D, Berger C, Cyrot-Lackmann F, Klein T and Lanco P 1993 *Phys. Rev. Lett.* **70** 3915
[3] Poon S J 1992 *Adv. Phys.* **41** 303
Kimura K and Takeuchi S 1991 *Quasicrystals: The State of the Art* ed D P DiVincenzo and P J Steinhardt (Singapore: World Scientific) p 313
[4] Belin E and Danhkázi Z 1993 *J. Non-Cryst. Solids* **153–154** 298
[5] Mizutani U, Kamiya A, Matsuda T, Kishi K and Takeuchi S 1991 *J. Phys.: Condens. Matter* **3** 3711
[6] Hippert F, Kandel L, Calvayrac Y and Dubost B 1992 *Phys. Rev. Lett.* **69** 2086
[7] Pierce F S, Bancel P A, Biggs B D, Guo Q and Poon S J 1993 *Phys. Rev.* B **47** 5670
[8] Fujiwara T and Yokokawa T 1991 *Phys. Rev. Lett.* **66** 333
Hafner J and Krajčí M 1993 *Phys. Rev.* B **47** 11 795
[9] Hume-Rothery W 1926 *J. Inst. Met.* **35** 295
Hume-Rothery W and Raynor G V 1954 *The Structure of Metals and Alloys* (London: Institute of Metals)
[10] Bancel P A and Heiney P A 1986 *Phys. Rev.* B **33** 7917
Smith A P and Ashcroft N W 1987 *Phys. Rev. Lett.* **59** 1365
Vaks V G , Kamyshenko V V and Samolyuk G D 1988 *Phys. Lett.* A **132** 131
Friedel J 1992 *Phil. Mag.* B **65** 1125 and references therein
[11] Bessière M, Quivy A, Lefebvre S, Devaud-Rzepski J and Calvayrac Y 1991 *J. Physique* I **1** 1823
[12] Gayle F W, Shapiro A J, Biancaniello F S and Boettinger W J 1992 *Metall. Trans.* A **23** 2409
[13] Gratias D, Calvayrac Y, Devaud-Rzepski J, Faudot F, Harmelin M, Quivy A and Bancel P A 1993 *J. Non-Cryst. Solids* **153–154** 482
[14] Dénoyer F, Heger G, Lambert M, Audier M and Guyot P 1990 *J. Physique* **51** 651
[15] Quiquandon M, Quivy A, Devaud J, Faudot F, Lefebvre S, Bessière M and Calvayrac Y 1994 in preparation
[16] Faudot F 1993 *Ann. Chim.* **18** 445
[17] Lawther D W and Dunlap R A 1993 *J. Non-Cryst. Solids* **153–154** 45
[18] Shastri A, Borsa F, Goldman A I, Shield J E and Torgeson D R 1993 *J. Non-Cryst. Solids* **153–154** 347
[19] Stadnik Z M and Stroink G 1988 *Phys. Rev.* B **38** 10 447
Kataoka N, Tsai A P, Inoue A, Masumoto T and Nakamura Y 1988 *Japan. J. Appl. Phys.* **27** L1125

Stadnik Z M, Stroink G, Ma H and Williams G 1989 *Phys. Rev.* B **39** 9797
Teillet J and Bouchet-Fabre B 1990 *Hyperfine Interact.* **55** 1077
Müller F, Rosenberg M, Liu W and Köster U 1991 *Mater. Sci. Eng.* A **134** 900
Chien C L and Lu M 1992 *Phys. Rev.* B **45** 12793
Ping J Y, Raincourt D G and Stadnik Z M 1992 *Hyperfine Interact.* **69** 493
Nasu S, Miglierini M, Ishihara K N and Shingu P H 1992 *J. Phys. Soc. Japan* **61** 3766
Eibschütz M, Lines M E, Chen H S and Thiel F A 1992 *Phys. Rev.* B **46** 491
Miglierini M and Nasu S 1993 *Mater. Trans. JIM* **34** 178

[20] Greneche J M and Varret F 1982 *J. Physique Lett.* **43** 233

[21] Brand R A, Pelloth J, Hippert F and Calvayrac Y 1994 *Hyperfine Interact.* at press

[22] Matsuo S, Nakano H, Ishimasa T and Fukano Y 1989 *J. Phys.: Condens. Matter* **1** 6893
Klein T, Berger C, Mayou D and Cryot-Lackmann F 1991 *Phys. Rev. Lett.* **66** 2907

[23] Drews A R, Rubinstein M, Stauss G H, Bennett L H and Swartzendruber L J 1993 *J. Alloys Compounds* **190** 189

[24] Le Caër G, Brand R A and Dubois J-M 1987 *Phil. Mag. Lett.* **56** 143
Eibschütz M, Lines M E, Chen H S, Waszczak J V, Papaefthymiou G and Frankel R B 1987 *Phys. Rev. Lett.* **59** 2443
Brand R A, Le Caër G and Dubois J-M 1990 *J. Phys.: Condens. Matter* **2** 6413
Lu M and Chien C L 1992 *Hyperfine Interact.* **71** 1525
Dunlap R A and Lawther D W 1993 *Mater. Sci. Eng.* R **10** 141 Lawther D W and Dunlap R A 1993 *J. Non-Cryst. Solids* **153–154** 49
Long G J, Grandjean F, Zhang X, Gibbons P C and Kelton K F 1993 *J. Non-Cryst. Solids* **153–154** 58

[25] David W I F 1986 *J. Appl. Crystallogr.* **19** 63

[26] Czjzek G, Fink J, Götz F, Schmidt H, Coey J M D, Rebouillat J P and Liénard A 1981 *Phys. Rev.* B **23** 2513

[27] Le Caër G and Brand R A 1992 *Hyperfine Interact.* **71** 1507

[28] Shenoy G K and Wagner F E (ed) 1978 *Mössbauer Isomer Shifts* (Amsterdam: North-Holland)

[29] Kaufmann E F and Vianden R J 1979 *Rev. Mod. Phys.* **51** 161

[30] Warren W W, Chen H S and Espinosa G P 1986 *Phys. Rev.* B **34** 4902
Shinohara T, Tsai A P and Masumoto T 1992 *J. Phys.: Condens. Matter* **4** 3043

[31] Yasuoka H, Soyama A, Kimura K and Takeuchi S 1986 *J. Phys. Soc. Japan* **55** 1058

[32] Carter G C, Bennett L H and Kahan D J 1977 *Metallic shifts in NMR* (Oxford: Pergamon)

[33] Burkov S E, Timusk T and Ashcroft N W 1992 *J. Phys.: Condens. Matter* **4** 9447

[34] Fujiwara T and Tsunetsugu H 1991 *Quasicrystals: The State of the Art* ed D P DiVincenzo and P J Steinhardt (Singapore: World Scientific) p 343

[35] Sadoc A, Berger C, Calvayrac Y 1993 *Phil. Mag.* B **68** 475

[36] Raynor A V 1949 *Prog. Met. Phys.* **1** 1

[37] Mayou D, Cyrot-Lackmann F, Trambly de Laissardière G and Klein T 1993 *J. Non-Cryst. Solids* **153–154** 412

[38] Wagner J L, Biggs B D and Poon S J 1990 *Phys. Rev. Lett.* **65** 203

[39] Dunlap R A 1993 *Phil. Mag. B* **67** 69

[40] Lemmerz U, Grushko B, Freiburg C and Jansen M 1994 *Phil. Mag. Lett.* **69** 141

[41] Lindqvist P, Berger C, Klein T, Lanco P, Cyrot-Lackmann F and Calvayrac Y 1993 *Phys. Rev.* B **48** 630